

Marquette University

e-Publications@Marquette

---

Biomedical Engineering Faculty Research and  
Publications

Biomedical Engineering, Department of

---

8-2010

## Local Hemodynamic Changes Caused by Main Branch Stent Implantation and Subsequent Side Branch Balloon Angioplasty in a Representative Coronary Bifurcation

Andrew R. Williams  
*Marquette University*

Bon-Kwon Koo  
*Seoul National University*

Timothy J. Gundert  
*Marquette University*

Peter J. Fitzgerald  
*Stanford University Medical Center*

John F. LaDisa Jr.  
*Marquette University*, john.ladisa@marquette.edu

Follow this and additional works at: [https://epublications.marquette.edu/bioengin\\_fac](https://epublications.marquette.edu/bioengin_fac)



Part of the [Biomedical Engineering and Bioengineering Commons](#)

---

### Recommended Citation

Williams, Andrew R.; Koo, Bon-Kwon; Gundert, Timothy J.; Fitzgerald, Peter J.; and LaDisa, John F. Jr., "Local Hemodynamic Changes Caused by Main Branch Stent Implantation and Subsequent Side Branch Balloon Angioplasty in a Representative Coronary Bifurcation" (2010). *Biomedical Engineering Faculty Research and Publications*. 496.

[https://epublications.marquette.edu/bioengin\\_fac/496](https://epublications.marquette.edu/bioengin_fac/496)

Marquette University

**e-Publications@Marquette**

***Biomedical Engineering Faculty Research and Publications/College of Engineering***

***This paper is NOT THE PUBLISHED VERSION; but the author's final, peer-reviewed manuscript.*** The published version may be accessed by following the link in the citation below.

*Journal of Applied Physiology*, Vol. 109, No. 2 (August 2010): 532-540. [DOI](#). This article is © American Physiological Society and permission has been granted for this version to appear in [e-Publications@Marquette](#). American Physiological Society does not grant permission for this article to be further copied/distributed or hosted elsewhere without the express permission from American Physiological Society.

# Local Hemodynamic Changes Caused by Main Branch Stent Implantation and Subsequent Virtual Side Branch Balloon Angioplasty in A Representative Coronary Bifurcation

Andrew R. Williams

Department of Biomedical Engineering, Marquette University, Milwaukee, Wisconsin

Bon-Kwon Koo

Center for Cardiovascular Technology, Stanford University Medical Center, Stanford, California  
Seoul National University College of Medicine, Seoul, Korea

Timothy J. Gundert

Department of Biomedical Engineering, Marquette University, Milwaukee, Wisconsin

Peter J. Fitzgerald

Center for Cardiovascular Technology, Stanford University Medical Center, Stanford, California

John F. LaDisa Jr.

Department of Biomedical Engineering, Marquette University, Milwaukee, Wisconsin  
Department of Medicine, Medical College of Wisconsin  
Department of Pediatrics, Children's Hospital of Wisconsin, Milwaukee, Wisconsin

## Abstract

Abnormal blood flow patterns promoting inflammation, cellular proliferation, and thrombosis may be established by local changes in vessel geometry after stent implantation in bifurcation lesions. Our objective was to quantify altered hemodynamics due to main vessel (MV) stenting and subsequent virtual side branch (SB) angioplasty in a coronary bifurcation by using computational fluid dynamics (CFD) analysis. CFD models were generated from representative vascular dimensions and intravascular ultrasound images. Time-averaged wall shear stress (TAWSS), oscillatory shear index (OSI), and fractional flow reserve (FFR) were quantified. None of the luminal surface was exposed to low TAWSS ( $<4$  dyn/cm<sup>2</sup>) in the nondiseased bifurcation model. MV stenting introduced eccentric areas of low TAWSS along the lateral wall of the MV. Virtual SB angioplasty resulted in a more concentric region of low TAWSS in the MV distal to the carina and along the lateral wall of the SB. The luminal surface exposed to low TAWSS was similar before and after virtual SB angioplasty (rest: 43% vs. 41%; hyperemia: 18% vs. 21%) and primarily due to stent-induced flow alterations. Sites of elevated OSI ( $>0.1$ ) were minimal but more impacted by general vessel geometry established after MV stenting. FFR measured at a jailed SB was within the normal range despite angiographic stenosis of 54%. These findings indicate that the most commonly used percutaneous interventional strategy for a bifurcation lesion causes abnormal local hemodynamic conditions. These results may partially explain the high clinical event rates in bifurcation lesions.

Stents are implanted in 70–90% of the 1.3 million percutaneous coronary interventions performed annually in the U.S. (1), and 18–20% of lesions involve bifurcations (32). Attempts to treat coronary bifurcation lesions with multiple stents have failed to conclusively prove the benefit of a systematic two-stenting strategy (4, 6), and data regarding long-term outcomes for dedicated bifurcation stents, although promising, are still forthcoming (5, 12, 21, 25, 39). Treatment of bifurcation lesions therefore favors main vessel (MV) stenting with provisional side branch (SB) balloon angioplasty or stenting (33).

MV stenting often results in the aggravation of SB ostial lesions. Shifting of plaque from the MV, the presence of stent struts in the ostium, and vasospasm have all been thought to cause this SB narrowing (22). However, recent studies have demonstrated that a stent-induced increase in lumen diameter of the distal MV forces the position of the carina into the SB ostium (37, 38) and this carina shift is the main mechanism of the SB narrowing after MV stent implantation. This finding is particularly interesting considering the influence of this unique change in vascular geometry on local hemodynamic alterations and on the physiological significance of ostial stenosis (30, 38).

Abnormal patterns of blood flow are known to be associated with inflammation, cellular proliferation, and thrombosis (3). Plaque and neointimal hyperplasia tend to form in bifurcations within the coronary arteries where normal patterns of blood flow are disturbed (23, 34). Studies have shown that altered geometry and associated blood flow disturbances established after stenting can also influence restenosis (9, 13, 20, 24, 31, 40). Even when proliferative responses to these altered hemodynamics are completely blocked by drug-eluting stents (DES), abnormal flow patterns can be a possible cause of thrombosis (3, 29). Despite the putative link between altered hemodynamics and clinically significant consequences, few studies to date have examined the influence of commonly used bifurcation stenting techniques on local blood flow distributions. Computational fluid dynamics (CFD) is an advanced simulation technique that utilizes measured vascular geometry and hemodynamic data, making it well-suited for this purpose. The objective of the present investigation was to

quantify altered hemodynamics due to MV stenting with and without subsequent virtual SB angioplasty that computationally removed struts from the ostium of a representative coronary bifurcation with CFD analysis.

## MATERIALS AND METHODS

### Creation of Idealized Left Anterior Descending Coronary Artery-Diagonal Branch Bifurcation Models

A nondiseased idealized bifurcation model was created with a typical bifurcation angle and Finet's law (8, 26). The location of the carina, SB ostial area, and distal MV dimensions after MV stent implantation and SB angioplasty were then altered based on the concept of carina shift (38) and intravascular ultrasound (IVUS) images (Fig. 1). After vascular dimensions were determined, a part document was created with Solid Edge computer-aided design software (Siemens, Plano, TX). Cross sections were sketched along the axis of each vessel. Protrusion and rounding functions were utilized within the software to join the cross sections and blend the intersection of the vessels, respectively. Stented vessels incorporated the *Express<sup>2</sup>* stent design (Boston Scientific, Natick, MA). Stents were generated from a hollow tube with the appropriate strut thickness. A sketch with the linkage pattern and strut dimensions was wrapped onto the tube in Solid Edge. The stent pattern was then cut from the tube with the normal cutout command, and the stent pattern was propagated radially and axially before excess material on the ends of the stent was removed. A Boolean intersection command was then implemented to subtract the stent from the lumen, thereby generating the potential region for blood flow within the bifurcation after MV stenting and virtual SB balloon angioplasty. For the poststent model, best- and worst-case stent orientations were constructed and simulated. For the best orientation, the stent was rotated and translated along the axis of the vessel so as little stent material as possible obstructed the SB ostium. Conversely, the worst-case representation oriented the stent to deliberately position struts at the entry of the SB. For the post-virtual angioplasty model, all stent struts were removed from the ostium of the SB (Fig. 1). Additional simulations were also conducted for the post-stent and virtual SB balloon angioplasty cases in the absence of a stent in order to isolate the independent hemodynamic contributions of struts compared with general vessel geometry.

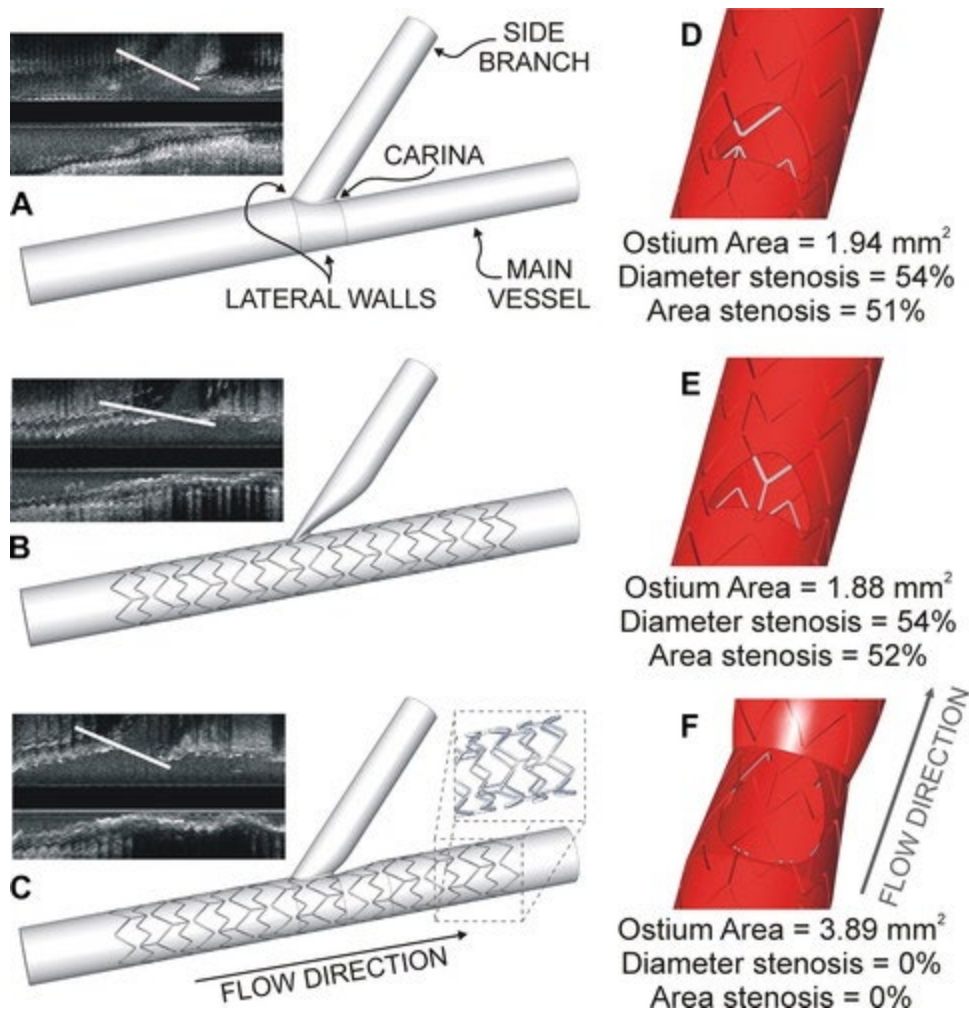


**Fig. 1.** Representative intravascular ultrasound (IVUS) images, corresponding idealized computational fluid dynamics (CFD) vascular representations, and the location of stent struts within the side branch (SB) ostium. Finet's law and a  $46^\circ$  bifurcation angle were used to create a nondiseased idealized bifurcation model (A). The location of the carina, SB ostial area and distal main vessel (MV) dimensions were then altered based on IVUS images and the concept of carina shift to create the poststenting (B) and SB balloon angioplasty (C) models. White lines on the IVUS images denote the angle between the carina and the junction of the MV and SB along the lateral wall of the bifurcation. In poststenting cases, the stent was rotated and translated along the axis of the vessel so as little stent material as possible obstructed the SB ostium (D), and so struts were deliberately positioned at the entry of the SB (E). Stent struts were removed from the ostium for the post-virtual SB angioplasty case (F). Locations mentioned frequently and the primary direction of blood flow have been labeled for clarity.

## CFD Simulations

### *Inflow conditions and flow distributions to model branches.*

Arteries were assumed to be rigid and subjected to blood flow velocity waveforms obtained from a canine left anterior descending coronary artery (LAD) under normal resting and hyperemic conditions shown in Fig. 2 and as previously described (18). Resting and hyperemic inflow waveforms (Reynolds number  $\sim 90$  and  $240$ , respectively) were imposed as temporally varying Womersley velocity profiles ( $\alpha = 2.9$  and  $2.6$ , respectively) with the cvSim CFD software package (Cardiovascular Simulation, Mountain View, CA; [www.cvsim.com](http://www.cvsim.com)). The distribution of blood flow between the distal LAD and diagonal (Dg) outlets was calculated by assuming that wall

shear stress (WSS) is the same in the distal MV and SB. The resulting distribution of blood flow to the LAD and Dg branches was 64% and 36%, respectively, for all models.

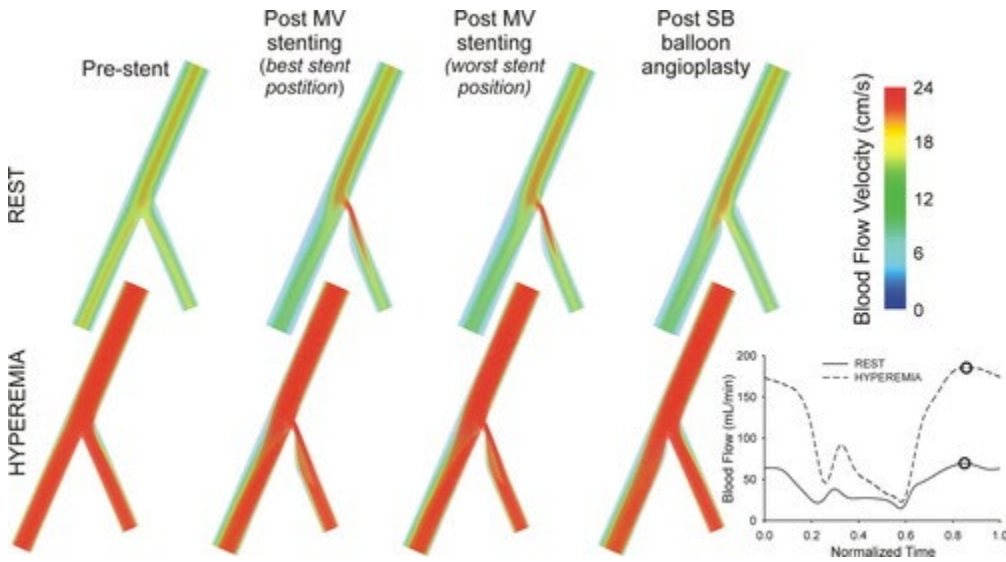


**Fig. 2.** Volume rendering of changes in blood flow velocity magnitude introduced by bifurcation stenting. Blood flow velocity nearest the wall (values  $<0.1$  cm/s) was made transparent to reveal velocity magnitude during maximum blood flow under resting (*top*) and hyperemic (*bottom*) flow conditions in the MV and SB. Inflow waveform contours previously obtained from a canine left anterior descending coronary artery under normal resting and hyperemic conditions during continuous adenosine infusion are shown at *bottom right* and were imposed at the inlet of CFD models. The temporal locations for volume renderings are denoted by circles.

*Outlet conditions.*

Outlet boundary conditions for the coronary vasculature are more difficult to prescribe than in other vascular beds since pronounced resistance introduced by ventricular contraction results in a nonlinear and time-varying system (2). However, previous work has demonstrated that linearity and time invariance can be assumed and the behavior of the downstream vasculature in the absence of ventricular contraction can be estimated with a three-element windkessel (i.e.,  $R_c$ ,  $C$ ,  $R_d$ ) approximation (36). Parameters utilized for resting and hyperemia conditions are provided in Table 1, and the details of how these values were obtained are provided in the online data supplement.<sup>1</sup>

Table 1. CFD simulation parameters

Flow Condition	Outlet Branch	$R_t$ , dyn·s·cm <sup>-5</sup>	$R_c$ , dyn·s·cm <sup>-5</sup>	$C$ , cm <sup>5</sup> /dyn	$R_d$ , dyn·s·cm <sup>-5</sup>
Rest	LAD	194,900	15,690	2.24E-06	179,300
	Dg	346,200	23,000	1.26E-06	323,200
Hyperemia	LAD	73,660	18,410	1.60E-05	55,250
	Dg	130,800	27,000	9.01E-06	103,800

CFD, computational fluid dynamics; LAD, left anterior descending coronary artery; Dg, diagonal branch;  $R_c$ , characteristic impedance;  $C$ , capacitance;  $R_d$ , distal resistance;  $R_t$ , total vascular resistance in the absence of ventricular contraction (i.e., 0 Hz impedance,  $Z_0$ ) by the impulse response method of Van Huis et al. (36).

*Additional simulation parameters.*

Blood was assumed to behave as a Newtonian fluid with a density of 1.06 g/cm<sup>3</sup> and dynamic viscosity of 4 cP. Five cardiac cycles were run to ensure that simulation results were periodic. Periodicity was assumed when the

maximum errors between equivalent points in successive cardiac cycles for pressure and flow were  $<1$  mmHg and  $1 \text{ mm}^3/\text{s}$ , respectively. Stented bifurcation models were discretized with a commercially available adaptive mesh generation program (MeshSim, Simmetrix, Clifton Park, NY). Final mesh edge sizes were adequate to resolve microscopic flow in the neighborhood of struts, and simulations were scrutinized to ensure that results were independent of the number of mesh elements in each model (see online data supplement for additional details).

## CFD Analysis

CFD simulations were performed by using a stabilized finite element method to solve the equations for conservation of mass (continuity) and balance of fluid momentum (Navier-Stokes) (7). After verification that simulation results were mesh independent and replicated aimed blood pressure and flow distributions, time-averaged wall shear stress (TAWSS), oscillatory shear index (OSI), and fractional flow reserve (FFR) were quantified. Previous studies have demonstrated that distributions of TAWSS  $<4 \text{ dyn/cm}^2$  and high temporal oscillations in WSS quantified by OSI are associated with cellular proliferation, intimal thickening, and inflammation (10). TAWSS and OSI were therefore calculated as previously described (35). An automated computer program was written to quantify the area of simulation results containing TAWSS  $<4 \text{ dyn/cm}^2$ . Lower OSI values indicate that WSS is oriented predominantly in the primary direction of blood flow, while a value of 0.5 is indicative of bidirectional WSS with a time-averaged value of 0 throughout the cardiac cycle. The area of the lumen surfaces containing OSI  $>0.1$  was also quantified with the procedure described for low TAWSS.

FFR is a physiological parameter representing the fraction of maximal myocardial flow that can be maintained in the presence of an epicardial coronary stenosis (27, 28). In practice, FFR can be obtained by the ratio of distal coronary pressure and proximal aortic pressure. In this study, FFR was calculated with transient pressure and flow values queried from converged simulation results at the inlet and 1 cm distal to the bifurcation in the SB.

## RESULTS

### Blood Flow Velocity

Images of blood flow velocity for various stages of the cardiac cycle during resting and hyperemia are provided for each model in the online data supplement. Figure 2 shows maximum blood flow velocity during the cardiac cycle and provides a good summary of important features throughout the entire cardiac cycle. Under resting blood flow conditions, velocity patterns follow those typical for bifurcations: velocity profiles are skewed toward the carina, resulting in higher velocity along the medial walls and lower velocity on the outer lateral walls (Fig. 3). MV stenting introduces a pronounced velocity jet in the SB with vortices extending from the jailed struts into the SB and causing eccentric areas of low velocity on the MV lateral wall away from the carina and in the SB distal to the carina. Virtual SB angioplasty introduces a more concentric region of low velocity in the MV distal to the carina and an area of low velocity in the SB lateral wall opposite the carina. These changes are accentuated in the corresponding bottom rows of Figs. 2 and 3, revealing peak blood flow velocity under hyperemic conditions.

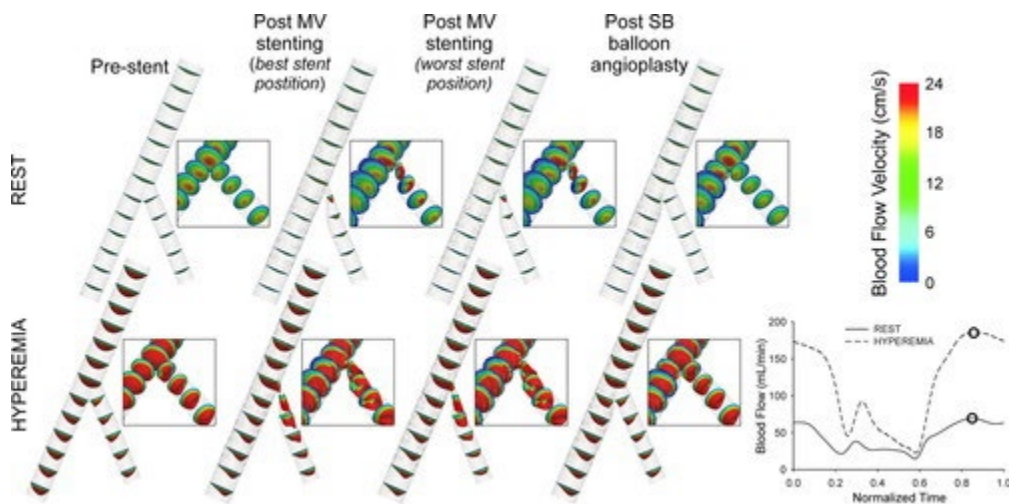


**Fig. 3.** Blood flow velocity profiles every 2.5 mm along the length of idealized coronary bifurcations. *Insets* offer zoomed versions of velocity profiles near the carina. Inflow waveform contours previously obtained from a canine left anterior descending coronary artery under normal resting and hyperemic conditions during continuous adenosine infusion are shown at *bottom right* and were imposed at the inlet of CFD models. The temporal locations for velocity profiles are denoted by circles.

### Indexes of Wall Shear Stress

Distributions of TAWSS and OSI are provided in Figs. 4 and 5, respectively. None of the luminal surface was exposed to TAWSS  $< 4$  dyn/cm<sup>2</sup> under resting or hyperemic conditions. Stenting introduced areas of low TAWSS along the struts at rest that persisted during hyperemia. Regions of low TAWSS were particularly pronounced eccentrically along the lateral wall of the proximal MV. Virtual SB balloon angioplasty introduced a more concentric region of low TAWSS in the MV distal to the carina and a region of low TAWSS along the lateral wall of the SB. Despite this regional variation in the location of low TAWSS, the total area of the luminal surface exposed to TAWSS  $< 4$  dyn/cm<sup>2</sup> was similar before and after SB balloon angioplasty (poststenting vs. post-SB angioplasty; rest: 43% vs. 41%; hyperemia: 18% vs. 21%; Fig. 6A). The local TAWSS behavior for each vessel is also depicted at four circumferential and axial locations in the online data supplement, where additional quantification of low TAWSS in the proximal and distal MV and SB is also provided.

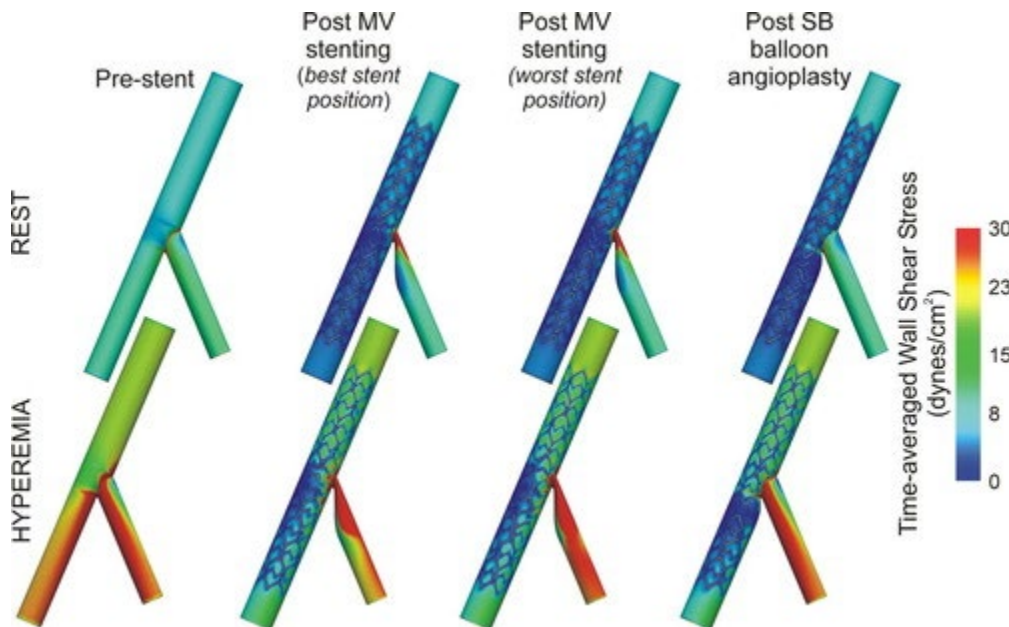


**Fig. 4.** Changes in time-averaged wall shear stress (TAWSS) introduced by bifurcation stenting: distributions of TAWSS under resting (*top*) and hyperemic (*bottom*) flow conditions in the MV and SB. The best stent position indicates that the least number of struts obstructed the SB ostium, and the worst stent position deliberately positioned the greatest amount of struts at the entry of the SB. All struts were removed from the ostium of the SB for the post-virtual angioplasty model.

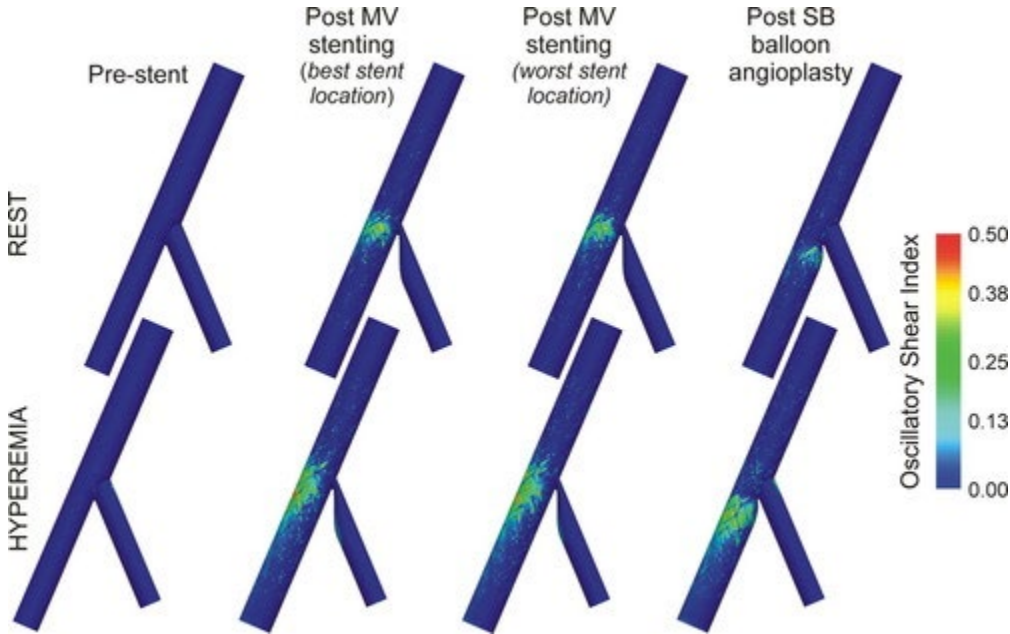


**Fig. 5.** Changes in oscillatory shear index (OSI) introduced by bifurcation stenting: distributions of OSI under resting (*top*) and hyperemic (*bottom*) flow conditions in the MV and SB. The best stent position indicates that the least number of struts obstructed the SB ostium, and the worst stent position deliberately positioned the greatest amount of struts at the entry of the SB. All struts were removed from the ostium of the SB for the post-virtual angioplasty model.

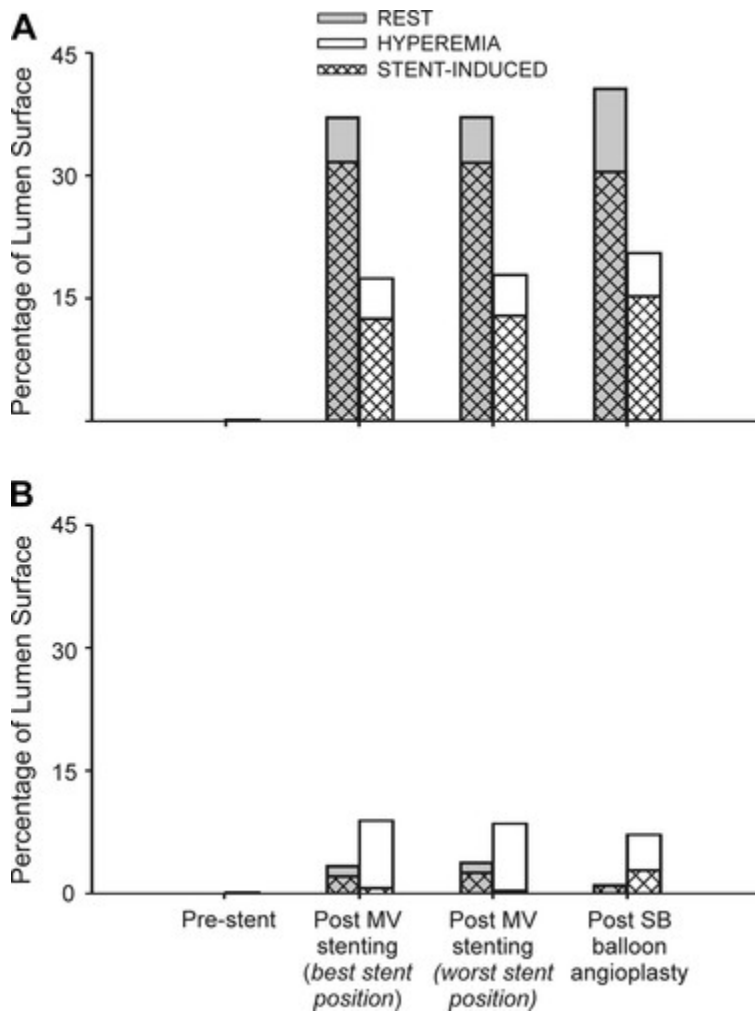


**Fig. 6.** Quantification of low wall shear stress and elevated OSI: % of the luminal surface exposed to TAWSS <4 dyn/cm<sup>2</sup> (A) and OSI >0.1 (B) during resting and hyperemic conditions. Cross-hatched portions of columns indicate % of low-TAWSS or high-OSI vessel area caused by the presence of the stent, compared with the general geometry of the vessel, for each simulation.

Elevated OSI is also absent in the idealized bifurcation before stenting, and only 4% and 8% of the luminal surface was exposed to elevated OSI during resting and hyperemic conditions, respectively, after MV stenting regardless of the amount (i.e., area) of struts within the ostium. Virtual SB balloon angioplasty reduced the total area of the luminal wall exposed to OSI > 0.1 at rest (1%) but had little impact during hyperemia (7%, Fig. 6B).

The presence and intricacies of the stent accounted for the majority of the vessel wall area subjected to low TAWSS under resting and hyperemia conditions (Fig. 6A). In contrast, there were relatively few strut-induced separation regions (areas of OSI >0.1) established after MV stenting (~5% of the vessel area) and areas were further reduced after virtual SB angioplasty. However, regions of elevated OSI during hyperemia occur primarily in response to overall modifications in vessel geometry, even after restoration of the carina to its original location (Fig. 6B).

### Fractional Flow Reserve

FFR in the SB as result of MV stenting-induced stenosis, or by partial occlusion of the ostium by stent struts, ranged from 0.95 to 0.99. The severity of stent struts present in the ostium had a greater impact on FFR than

shifting of the carina (poststent best and worst cases: 0.98 and 0.95, respectively; post-SB virtual angioplasty: 0.99), but all values were well above the clinically significant criterion of 0.75.

## DISCUSSION

The bifurcation lesion is still one of the most challenging lesion subsets in the field of percutaneous coronary intervention (5, 12, 21, 25, 32). As alterations in indexes of WSS are reported to be associated with the progression of atherosclerosis (23), it is important to understand local, potentially adverse, changes in these hemodynamic indexes as a result of interventions in order to develop better strategies and devices. However, there are few studies of hemodynamic changes associated with interventional strategies for bifurcation lesions to date. The present investigation offers several unique aspects applicable to this area: 1) The findings demonstrate that CFD can be used to quantify altered hemodynamics due to MV stenting and subsequent SB angioplasty in a coronary bifurcation with a realistic commercially available stent design and representative changes in local vascular geometry. 2) The outlet boundary conditions used allow for quantification of FFR, a clinical parameter routinely evaluated with application to interventional treatment planning. The importance of these methods is exemplified in the poststenting cases, where the severity of the SB ostium by visual inspection would have suggested a reduction in FFR. This is not the case because of the more physiological boundary conditions available in the software utilized for this CFD investigation. 3) Local quantification methods were employed to quantify the amount of flow alterations due to overall vessel geometry versus the intricacies of stent struts, as well as to reveal circumferential and axial alterations in WSS indexes (shown in the online data supplement), 4) The results theoretically demonstrate that there may not be a benefit to SB intervention from a fluid dynamics perspective.

The vascular dimensions used for our nondiseased bifurcation model are based on Finet's law, and the fractal ratio between mother and daughter vessel diameters was 0.678 (8). CFD revealed that none of the luminal surface was exposed to low TAWSS or elevated OSI under both resting and hyperemic conditions. Similar findings were found in a previous flow visualization study (30) encompassed by the resting and hyperemia cases here, suggesting that this ratio should be reestablished after intervention for bifurcation lesions to achieve hemodynamically favorable results.

Previous clinical trials have not shown distinctive benefits of systematic multistenting strategies. MV stenting with provisional SB intervention is therefore the most common approach for bifurcation lesions (5, 21, 33). In our study, idealized models before and after MV and SB angioplasty were created and CFD was performed for each model. Simple MV stenting across the bifurcating segment caused eccentric areas of low TAWSS and elevated OSI in the MV opposite the carina. This region experienced pronounced leukocyte adhesion, neointimal hyperplasia, and fibrin deposition in a previous chronic porcine study establishing a similar flow scenario in vivo by SB occlusion, assumed MV remodeling, and restoration of SB flow after 28 days (30). Importantly, our quantification revealed that the total area of low TAWSS was essentially the same after MV stenting and after virtual SB angioplasty. While virtual SB angioplasty restored carina position, it also caused concentric low TAWSS and high OSI in the distal MV due to slight repositioning of the carina within the MV. Thus, although post-SB angioplasty provides an excellent result in terms of patency, from a fluid dynamics perspective there are only modest differences, indicating that the potential for neointimal hyperplasia or thrombus formation may be unchanged. Although a post-kissing balloon inflation model was not tested in our study, the present investigation and the previous study discussed above indicate that overdilatation of the proximal MV segment associated with this technique will result in additional flow disturbances.

These findings are particularly interesting when coupled with transport of a drug-eluting agent after DES implantation. Kolachalama et al. (14) placed a slotted-tube DES at three MV positions within an idealized coronary bifurcation: proximal to the SB ostium, across the bifurcation entrance, and distal to the carina. Stent-

induced flow alterations proximal and distal to the bifurcation region were generally symmetric, producing concentric distribution patterns that varied along the length of the vessel as a result of flow extending the drug distribution downstream, but were modest in scale relative to the total transmural drug concentration beneath stent struts. However, the flow patterns established after MV stenting caused asymmetric drug deposition, with 8–15% greater concentration along the lateral wall opposite the flow divider when the stent was positioned across the SB ostium.

Bifurcation lesions are an independent risk factor for acute and late stent thrombosis (11, 17). Stenting along a major SB and complex two-stenting strategies are also known to be associated with higher risk of stent thrombosis. Although we cannot directly link hemodynamic disturbances and the risk of stent thrombosis based on the present work, it is plausible that the risk of thrombosis would be higher if portions of the MV are continuously exposed to low WSS as DES have nearly eliminated neointimal hyperplasia at the site of flow disturbance (29). The present investigation indicates that once the ratio between bifurcation vessel diameters is altered by overexpansion of the distal MV, SB angioplasty cannot improve the flow disturbance. This may be one possible mechanism for why SB angioplasty does not appear to reduce the risk of stent thrombosis.

Angiographic evaluation can overestimate functional significance in jailed SB lesions (15, 16). One of the mechanisms of this discrepancy may be the eccentric luminal narrowing of SB ostium due to carina relocation after MB stent implantation (37). In contrast to usual coronary stenotic lesions, the relation between angiographic luminal narrowing (percent diameter stenosis) and area stenosis in jailed SB lesions is not quadratic. In our carina shift model, FFR measured by both pressure and flow parameters were all within normal range despite angiographic stenosis of 54%.

The present results should be interpreted within the constraints of several potential limitations. Mesh independence was assumed when TAWSS at predetermined proximal and distal intrastrut regions changed  $<0.09 \text{ dyn/cm}^2$  between successive meshes. Meshes were created with unstructured and adapted tetrahedral elements by this approach and resulted in at least three elements along the thickness and width of stent struts. It is important to note that the adaptive meshing scheme applied in the present investigation places elements where they are most needed within the flow domain while inserting fewer elements where a coarse density is sufficient. This intelligent approach allows for results equivalent to those of isotropic meshes, but at a fraction of the computational time. Locally adapted elements also allowed us to resolve flow features for our intricate stent models at a level that would not be possible at most institutions using an isotropic approach.

Three-element windkessel outlet boundary conditions were applied because they most faithfully represent the aimed values of blood pressure and flow compared with other methods available. The implementation of these boundary conditions closely adheres to published values and known physiological and clinical principles. Their realism was further verified with additional simulations of a bifurcation vessel with a 75% decrease in diameter (90% area reduction) at the SB ostium. The FFR for this simulation was  $<0.75$ , consistent with measurements commonly obtained clinically for this level of stenosis. For resting cases presented here, flow distributions to the distal MV and SB remain unchanged after best- or worst-case stenting and virtual balloon angioplasty since any resulting residual stenoses in these cases do not represent critical reductions in area. For the hyperemic case, flow to the SB is reduced by 3–5% after stenting, and this reduction is alleviated after virtual SB balloon angioplasty. To our knowledge, clinical data as to local changes in flow or perfusion in these coronary vessels during hyperemia are not well documented. Importantly, if the flow distributions are different from rest under healthy hyperemic conditions, the results could differ from those presented. The C term in the  $R_c, C, R_d$  model accounts for the total arterial compliance (TAC) of the arterial system beyond the outlet of interest. Thus the use of rigid walls may result in a different value for the C parameters than would be used with deformable walls. However,  $>60\%$  of the TAC is in the thoracic aorta, so the use of rigid walls for coronary vessels in the present work likely resulted in C values similar to those that would be obtained with deformable walls.

The present models were created by using idealized representations of the coronary bifurcation lesion based on the carina shift model (38). In many of these cases, SB angioplasty can restore the carina to its original position as exemplified by the IVUS data shown in Fig. 1. Future work will include various clinical permutations of SB patency (i.e., carina position) since other mechanisms can also cause SB ostial lumen narrowing after MV stenting. Further studies are also needed to define the hemodynamic influence of different mechanisms of SB pinching after MV stenting. A bifurcation angle of  $46^\circ$  was also used here, but coronary branching patterns and vessel dimensions are heterogeneous, so results obtained from patient-specific CFD models could provide more realistic information.

Stent implantation into canine epicardial coronary arteries reduces regional vessel compliance to zero (18), suggesting that the present results may be generally applicable within the stent. However, the results may differ from those observed clinically, particularly immediately proximal and distal to the stent. In these proximal and distal transition regions, as well as intrastent regions, distributions of TAWSS would likely be lower than reported because of lower elastic moduli than the stent. Struts were not modeled as protruding into the wall, but rather as local strut obstructions. A modest and therefore negligible change in proximal MV stented diameter was assumed, and the proximal unstented transition region was not modeled. Similarly, although changes in diameter for the distal MV after stenting are included, the distal unstented transition region also was not modeled. Previous investigations indicate that these transitions would result in a more physiological stent-to-artery deployment ratio (19, 20) but relatively small changes in the resulting distributions of WSS and OSI at the proximal and distal edges of the stent, which were similar for all stented simulations.

Despite these limitations the present simulations reveal that areas of low TAWSS and, to a lesser extent, elevated OSI known to correlate with the potential clinical events are associated with the current clinical practice of provisional MV stenting and cannot be improved once established. While it is unclear whether low TAWSS or elevated OSI has a greater impact on restenosis, the present findings highlight an important distinction between the overall geometry of a vessel created after stenting and the specific impact of the stent while raising the intriguing question of how different stent designs may impact TAWSS in bifurcation lesions. The results may therefore partially explain why clinical event rates remain high in stented bifurcation lesions, and be amenable to improved future bifurcation stent designs. For example, stent linkages could be orienting within regions susceptible to plaque and hemodynamic alterations in a way that minimizes disturbances in near-wall velocity vectors and WSS. Shape optimization algorithms using a WSS cost function could also be applied to arrive at a favorable geometry. Moreover, it appears that reestablishing the diameter ratio of a natural healthy bifurcation after stenting may optimize local hemodynamics. Importantly, our results show that the overstretching of distal MV, which commonly occurs during a provisional strategy with conventional stents, can worsen local fluid dynamics and this cannot be restored by additional procedures such as SB angioplasty or kissing balloon inflation.

## GRANTS

This work was supported by National Science Foundation Grant CTS-0521602 (principal investigator: Dr. Scott Goldsborough, Marquette University Department of Mechanical Engineering) and the Marquette University Department of Biomedical Engineering. B.-K. Koo is the recipient of a research grant from the CardioVascular Research Foundation (CVRF), Korea.

## DISCLOSURES

No conflicts of interest, financial or otherwise, are declared by the author(s).

## FOOTNOTES

<sup>1</sup>Supplemental Material for this article is available online at the Journal website.

## ACKNOWLEDGMENTS

The authors recognize Dr. Nathan Wilson for technical assistance.

## AUTHOR NOTES

\*A. R. Williams and B.-K. Koo contributed equally to this work.

Address for reprint requests and other correspondence: J. F. LaDisa, Jr., Marquette Univ., 1515 West Wisconsin Ave., Rm. 206, Milwaukee, WI 53233 (e-mail: john.ladisa@marquette.edu).

## Supplemental data

- datasupp.pdf (1.07 MB)

## REFERENCES

1. American Heart Association. *Heart Disease and Stroke Statistics—2007 Update*. Dallas, TX: AHA, 2007.
2. Bovendeerd PH, Borsje P, Arts T, van De Vosse FN. Dependence of intramyocardial pressure and coronary flow on ventricular loading and contractility: a model study. *Ann Biomed Eng* 34: 1833–1845, 2006.
3. Chatzizisis YS, Coskun AU, Jonas M, Edelman ER, Feldman CL, Stone PH. Role of endothelial shear stress in the natural history of coronary atherosclerosis and vascular remodeling: molecular, cellular, and vascular behavior. *J Am Coll Cardiol* 49: 2379–2393, 2007.
4. Colombo A, Bramucci E, Sacca S, Violini R, Lettieri C, Zanini R, Sheiban I, Paloscia L, Grube E, Schofer J, Bolognese L, Orlandi M, Niccoli G, Latib A, Airolidi F. Randomized study of the crush technique versus provisional side-branch stenting in true coronary bifurcations: the CACTUS (Coronary Bifurcations: Application of the Crushing Technique Using Sirolimus-Eluting Stents) Study. *Circulation* 119: 71–78, 2009.
5. Colombo A, Moses JW, Morice MC, Ludwig J, Holmes DR, Spanos V, Louvard Y, Desmedt B, Di Mario C, Leon MB. Randomized study to evaluate sirolimus-eluting stents implanted at coronary bifurcation lesions. *Circulation* 109: 1244–1249, 2004.
6. Ferenc M, Gick M, Kienzle RP, Bestehorn HP, Werner KD, Comberg T, Kuebler P, Buttner HJ, Neumann FJ. Randomized trial on routine vs. provisional T-stenting in the treatment of de novo coronary bifurcation lesions. *Eur Heart J* 29: 2859–2867, 2008.
7. Figueroa CA, Vignon-Clementel IE, Jansen KE, Hughes TJR, Taylor CA. A coupled momentum method for modeling blood flow in three-dimensional deformable arteries. *Comput Methods Appl Mech Eng* 195: 5685–5706, 2006.
8. Finet G, Gilard M, Perrenot B, Rioufol G, Motreff P, Gavit L, Prost R. Fractal geometry of arterial coronary bifurcations: a quantitative coronary angiography and intravascular ultrasound analysis. *EuroIntervention* 3: 490–498, 2007.
9. Garasic JM, Edelman ER, Squire JC, Seifert P, Williams MS, Rogers C. Stent and artery geometry determine intimal thickening independent of arterial injury. *Circulation* 101: 812–818, 2000.
10. He X, Ku DN. Pulsatile flow in the human left coronary artery bifurcation: average conditions. *J Biomech Eng* 118: 74–82, 1996.
11. Iakovou I, Schmidt T, Bonizzoni E, Ge L, Sangiorgi GM, Stankovic G, Airolidi F, Chieffo A, Montorfano M, Carlino M, Michev I, Corvaja N, Briguori C, Gerckens U, Grube E, Colombo A. Incidence, predictors, and outcome of thrombosis after successful implantation of drug-eluting stents. *JAMA* 293: 2126–2130, 2005.
12. Ikeno F, Kim YH, Luna J, Condado JA, Colombo A, Grube E, Fitzgerald PJ, Park SJ, Yeung AC. Acute and long-term outcomes of the novel side access (SLK-View) stent for bifurcation coronary lesions: a multicenter nonrandomized feasibility study. *Catheter Cardiovasc Interv* 67: 198–206, 2006.

13. Kastrati A, Mehilli J, Dirschinger J, Pache J, Ulm K, Schuhlen H, Seyfarth M, Schmitt C, Blasini R, Neumann FJ, Schomig A. Restenosis after coronary placement of various stent types. *Am J Cardiol* 87: 34–39, 2001.
14. Kolachalama VB, Levine EG, Edelman ER. Luminal flow amplifies stent-based drug deposition in arterial bifurcations. *PLoS One* 4: e8105, 2009.
15. Koo BK, Kang HJ, Youn TJ, Chae IH, Choi DJ, Kim HS, Sohn DW, Oh BH, Lee MM, Park YB, Choi YS, Tahk SJ. Physiologic assessment of jailed side branch lesions using fractional flow reserve. *J Am Coll Cardiol* 46: 633–637, 2005.
16. Koo BK, Park KW, Kang HJ, Cho YS, Chung WY, Youn TJ, Chae IH, Choi DJ, Tahk SJ, Oh BH, Park YB, Kim HS. Physiological evaluation of the provisional side-branch intervention strategy for bifurcation lesions using fractional flow reserve. *Eur Heart J* 29: 726–732, 2008.
17. Kuchulakanti PK, Chu WW, Torguson R, Ohlmann P, Rha SW, Clavijo LC, Kim SW, Bui A, Gevorkian N, Xue Z, Smith K, Fournadjieva J, Suddath WO, Satler LF, Pichard AD, Kent KM, Waksman R. Correlates and long-term outcomes of angiographically proven stent thrombosis with sirolimus- and paclitaxel-eluting stents. *Circulation* 113: 1108–1113, 2006.
18. LaDisa JF, Hettrick DA, Olson LE, Guler I, Gross ER, Kress TT, Kersten JR, Warltier DC, Pagel PS. Coronary stent implantation alters coronary artery hemodynamics and wall shear stress during maximal vasodilation. *J Appl Physiol* 93: 1939–1946, 2002.
19. LaDisa JF, Olson LE, Guler I, Hettrick DA, Audi SH, Kersten JR, Warltier DC, Pagel PS. Stent design properties and deployment ratio influence indexes of wall shear stress: a three-dimensional computational fluid dynamics investigation within a normal artery. *J Appl Physiol* 97: 424–430, 2004.
20. LaDisa JF, Olson LE, Molthen RC, Hettrick DA, Pratt PF, Hardel MD, Kersten JR, Warltier DC, Pagel PS. Alterations in wall shear stress predict sites of neointimal hyperplasia after stent implantation in rabbit iliac arteries. *Am J Physiol Heart Circ Physiol* 288: H2465–H2475, 2005.
21. Lefevre T, Ormiston J, Guagliumi G, Schultheiss HP, Quilliet L, Reimers B, Brunel P, Wijns W, Buettner HJ, Hartmann F, Veldhof S, Miquel K, Su X, van der Giessen WJ. The Frontier stent registry: safety and feasibility of a novel dedicated stent for the treatment of bifurcation coronary artery lesions. *J Am Coll Cardiol* 46: 592–598, 2005.
22. Louvard Y, Lefevre T, Morice MC. Percutaneous coronary intervention for bifurcation coronary disease. *Heart* 90: 713–722, 2004.
23. Malek AM, Alper SL, Izumo S. Hemodynamic shear stress and its role in atherosclerosis. *JAMA* 282: 2035–2042, 1999.
24. Murata T, Hiro T, Fujii T, Yasumoto K, Murashige A, Kohno M, Yamada J, Miura T, Matsuzaki M. Impact of the cross-sectional geometry of the post-deployment coronary stent on in-stent neointimal hyperplasia: an intravascular ultrasound study. *Circ J* 66: 489–493, 2002.
25. Ormiston J, Webster M, El-Jack S, McNab D, Plaumann SS. The AST petal dedicated bifurcation stent: first-in-human experience. *Catheter Cardiovasc Interv* 70: 335–340, 2007.
26. Pflederer T, Ludwig J, Ropers D, Daniel WG, Achenbach S. Measurement of coronary artery bifurcation angles by multidetector computed tomography. *Invest Radiol* 41: 793–798, 2006.
27. Pijls NH, De Bruyne B, Peels K, Van Der Voort PH, Bonnier HJ, Bartunek JKJ, Koolen JJ. Measurement of fractional flow reserve to assess the functional severity of coronary-artery stenoses. *N Engl J Med* 334: 1703–1708, 1996.
28. Pijls NH, van Son JA, Kirkeeide RL, De Bruyne B, Gould KL. Experimental basis of determining maximum coronary, myocardial, and collateral blood flow by pressure measurements for assessing functional stenosis severity before and after percutaneous transluminal coronary angioplasty. *Circulation* 87: 1354–1367, 1993.
29. Richter Y, Edelman ER. Cardiology is flow. *Circulation* 113: 2679–2682, 2006.
30. Richter Y, Groothuis A, Seifert P, Edelman ER. Dynamic flow alterations dictate leukocyte adhesion and response to endovascular interventions. *J Clin Invest* 113: 1607–1614, 2004.
31. Rogers C, Edelman ER. Endovascular stent design dictates experimental restenosis and thrombosis. *Circulation* 91: 2995–3001, 1995.
32. Sharma SK, Kini AS. Coronary bifurcation lesions. *Cardiol Clin* 24: 233–246, 2006.
33. Steigen TK, Maeng M, Wiseth R, Erglis A, Kumsars I, Narbutė I, Gunnes P, Mannsverk J, Meyerdiereks O, Rotevatn S, Niemela M, Kervinen K, Jensen JS, Galloe A, Nikus K, Vikman S, Ravkilde J, James S, Aaroe J, Ylitalo A,

- Helqvist S, Sjogren I, Thayssen P, Virtanen K, Puhakka M, Airaksinen J, Lassen JF, Thuesen L. Randomized study on simple versus complex stenting of coronary artery bifurcation lesions: the Nordic bifurcation study. *Circulation* 114: 1955–1961, 2006.
34. Stone PH, Coskun AU, Kinlay S, Clark ME, Sonka M, Wahle A, Ilegbusi OJ, Yeghiazarians Y, Popma JJ, Orav J, Kuntz RE, Feldman CL. Effect of endothelial shear stress on the progression of coronary artery disease, vascular remodeling, and in-stent restenosis in humans: in vivo 6-month follow-up study. *Circulation* 108: 438–444, 2003.
35. Tang BT, Cheng CP, Draney MT, Wilson NM, Tsao PS, Herfkens RJ, Taylor CA. Abdominal aortic hemodynamics in young healthy adults at rest and during lower limb exercise: quantification using image-based computer modeling. *Am J Physiol Heart Circ Physiol* 291: H668–H676, 2006.
36. Van Huis GA, Sipkema P, Westerhof N. Coronary input impedance during cardiac cycle as determined by impulse response method. *Am J Physiol Heart Circ Physiol* 253: H317–H324, 1987.
37. Vassilev D, Gil R. Clinical verification of a theory for predicting side branch stenosis after main vessel stenting in coronary bifurcation lesions. *J Interv Cardiol* 21: 493–503, 2008.
38. Vassilev D, Gil RJ. Relative dependence of diameters of branches in coronary bifurcations after stent implantation in main vessel—importance of carina position. *Kardiol Pol* 66: 371–378, 2008.
39. Verheye S, Agostoni P, Dubois CL, Dens J, Ormiston J, Worthley S, Trauthen B, Hasegawa T, Koo BK, Fitzgerald PJ, Mehran R, Lansky AJ. 9-Month clinical, angiographic, and intravascular ultrasound results of a prospective evaluation of the Axxess self-expanding biolimus A9-eluting stent in coronary bifurcation lesions: the DIVERGE (Drug-Eluting Stent Intervention for Treating Side Branches Effectively) study. *J Am Coll Cardiol* 53: 1031–1039, 2009.
40. Yoshitomi Y, Kojima S, Yano M, Sugi T, Matsumoto Y, Saotome M, Tanaka K, Endo M, Kuramochi M. Does stent design affect probability of restenosis? A randomized trial comparing Multilink stents with GFX stents. *Am Heart J* 142: 445–451, 2001.